

An *in silico* model of the alternative oxidase

Shu-Ying Marissa Pang, Stephen Tristram and Simon Brown

School of Human Life Sciences, University of Tasmania, Locked Bag 1320, Launceston, Tasmania 7250, Australia

Simon.Brown@utas.edu.au

ABSTRACT

The alternative oxidase (AOX) is a member of the family of di-iron proteins, in which the catalytic centre consists of a pair of iron atoms ligated by carboxylate (aspartate and glutamate) and histidine ligands within a four helix bundle. Recently sequenced bacterial AOXs are homologues of the rubrerythrin domains of rubrerythrin and nigerythrin and so the crystal structure of *Desulfovibrio vulgaris* rubrerythrin (PDB accession code 1S2Z) was used as the basis for a simple model of AOX. The putative iron ligands were identified by analysis of their distribution in other di-iron proteins and protein sequence analysis and the putative quinone binding site was identified by sequence analysis. The pattern of hydropathy of the four helices implies that AOX is partially embedded in the membrane and that the quinone binding site is located on the most hydrophobic helix opposite residues associated with mutations conferring inhibitor resistance. These results may be used for further analysis using structure prediction software and subsequent site-directed mutagenesis of the putative quinone binding site, the aspartate residue involved in stabilising the di-iron histidine ligands and other physically significant residues.

INTRODUCTION

The alternative oxidase (AOX) reduces oxygen to water using ubiquinol (UQH₂) as an electron donor, but does not contribute to the electrochemical potential for protons across the inner mitochondrial membrane. The enzyme is not inhibited by cyanide, but is sensitive to compounds such as salicylhydroxamic acid (SHAM), disulfiram, aurachins and *n*-alkyl-gallates. Alternative oxidases are thought to be monomeric or homodimeric members of the family of di-iron proteins. While AOX requires iron to function [24], neither the reduced nor the oxidised forms of the enzyme exhibit any electron paramagnetic resonance (EPR) signals. However, a partially oxidised form of AOX has a characteristic EPR spectrum, presumably arising from the mixed-valence form (Fe(II)/Fe(III)) of the enzyme [7]. The mixed-valence state of other members of the di-iron family exhibit similar EPR spectra, but neither the oxidised nor the reduced forms of these proteins have EPR spectra [4, 22, 29].

Di-iron proteins are characterised by a pair of iron atoms ligated by carboxylate (aspartate and glutamate) and histidine ligands within a four helix bundle [19, 20]. Members of the family generate tyrosine radicals (ribonucleotide reductase), hydroxylate hydrocarbons (methane monooxygenase), desaturate fatty acids (Δ^9 -acyl carrier protein desaturase), reversibly bind O₂ (hemerythrin), hydrolyse phosphate esters (acid phosphatase), mineralise iron (bacterioferritin), transfer electrons (rubrerythrin and nigerythrin) and reduce nitric oxide (nitric oxide reductase) [19, 20, 36]. All of these, except nitric oxide reductase and acid phosphatase, bind O₂ and, of the remainder, methane monooxygenase and ribonucleotide reductase are not monomeric or homo-oligomeric. The Δ^9 -acyl carrier protein desaturases are

either integral membrane proteins, in which the di-iron centre is likely to be ligated by histidine ligands, or soluble proteins that react with ferredoxin and have a carboxylate-histidine ligated di-iron centre [12]. Only hemerythrin, rubrerythrin, nigerythrin and bacterioferritin bind oxygen and are homo-oligomeric members of the di-iron family, like AOX.

Rubrerythrin, nigerythrin, hemerythrin and bacterioferritin have very similar structures in which four helices surround the di-iron centre and the six ligands to the iron atoms are characteristically distributed along the length of the polypeptide (Figure 2). Rubrerythrin and nigerythrin have two distinct iron sites: a rubredoxin-like iron-sulphur centre in the rubredoxin domain and a rubrerythrin domain, containing a di-iron site [28]. Hemerythrin is a homo-octamer in which the iron atoms are ligated by five histidine residues, aspartate and glutamate residues and a water molecule [34, 35]. Bacterioferritin has 24 identical subunits, in which each monomer is a four α -helix bundle [17] containing a di-iron centre, and haem groups are ligated by methionine residues from adjacent subunits [21].

The structure of AOX has not yet been determined, but based on hydropathy analysis, Moore *et al.* [25] suggested that the enzyme has two transmembrane helices connected by a helix in the intermembrane space (Figure 1A). Subsequently, Andersson and Nordlund [3] proposed that AOX is an interfacial rather than an integral protein, largely based on the distribution of the putative ligands to the di-iron centre (Figure 1B). In other di-iron proteins, the iron ligands are provided by E-X-X-H motifs, of which there are several in the AOX sequences currently available. Moore *et al.* [25] based their structure on a C-terminal E₂₇₀-X-X-H motif which is not completely conserved (residue numbers are those

specified in the original reference), whereas Andersson and Nordlund [3] made use of a central E₂₁₇-X-X-H motif which is inconsistent with the two transmembrane helices of the Moore model [25]. Some support for the interfacial model was provided by Albury *et al.* [1] who generated a mutation (E217A) that inactivated the enzyme.

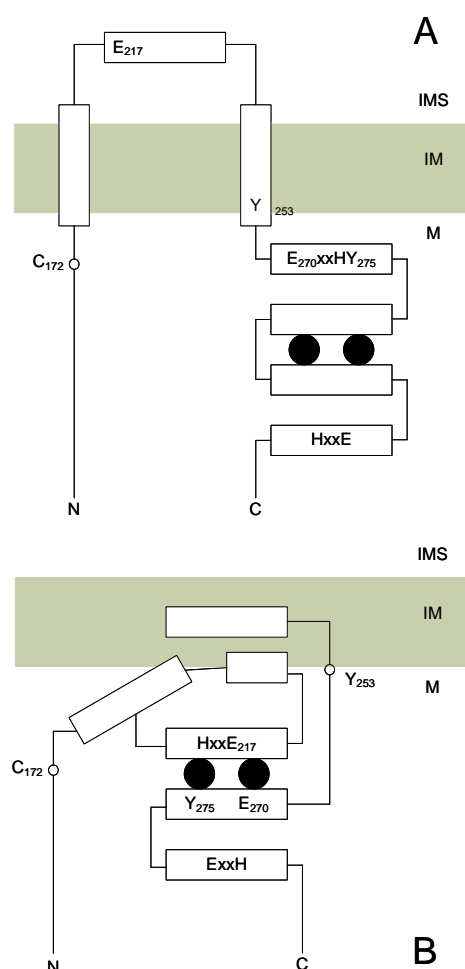


Figure 1. Transmembrane (A) and interfacial (B) models of the structure of AOX. The transmembrane model (A) was proposed by Moore *et al.* [25, 33], the interfacial model (B) was proposed by Andersson and Nordlund [3]. The residues are numbered according to the *Sauromatum guttatum* sequence [30], the filled circles represent the iron atoms and the rectangles represent the proposed helical regions. The iron-binding motifs (E-X-X-H) are also indicated. Mutations of the AOX as reported by Albury *et al.* [1] are indicated by numbered residues. IMS – intermembrane space; IM – inner membrane; M – matrix.

In addition to the O₂-binding di-iron site, there is also a quinone-binding site in AOX. Moore *et al.* [2, 25, 33] suggested that several residues at the matrix end of the two transmembrane helices, including Y₂₅₃, might be involved in quinone binding by analogy with the bacterial photosynthetic reaction centre [2, 8]. Berthold [6] observed that mutations affecting F₂₁₅, M₂₁₉ or G₃₀₃ in the *Arabidopsis thaliana* AOX led to SHAM resistance. Interestingly, G₃₀₃ is located in the poorly

conserved C-terminal region of the protein and a mutation affecting this residue (G303E) increased the I₅₀ for SHAM 4.6-fold, whereas mutations adjacent to the highly conserved E₂₂₄-E-E region (F215L, M219I and M219V) increased the I₅₀ for SHAM only 1.5-fold [6]. A Y275F mutation inactivated the *S. guttatum* AOX [1], but it is not clear whether this highly conserved residue is involved in electron transfer or quinone binding. In the *S. guttatum* and *A. thaliana* AOXs, most of the mutations so far reported have affected residues located in conserved regions, with the exception of C₁₇₂ (in *S. guttatum*) and F₂₁₅, F₂₁₉ and G₃₀₃ (in *A. thaliana*).

Here, an alternative structural model of AOX based on the rubrerythrin domain of the *Desulfovibrio vulgaris* rubrerythrin crystal structure (1S2Z, [18]) is described. The putative quinone binding site identified is close to the di-iron centre, perhaps consistent with efficient electron transfer. This model is consistent with an interfacial location in which the enzyme is partially embedded in the membrane.

MATERIALS AND METHODS

Alternative oxidase amino acid sequences from *Photobacterium profundum*, *Photobacterium* sp., *Vibrio fischeri*, *V. angustum*, *Erythrobacter* sp., *Thiobacillus denitrificans*, *Novosphingobium aromaticivorans*, *Cryptococcus neoformans* var. *neoformans*, *Yarrowia lipolytica*, *Neurospora crassa*, *Aspergillus oryzae*, *Candida maltosa* AOX 1a, *C. maltosa* AOX 1b, *C. albicans* AOX 1a and *C. albicans* AOX 1b (accession numbers ZP_01222260.1, ZP_01159533.1, AAW85073.1, ZP_01234787.1, ZP_01041525.1, YP_315688.1, ABD26016.1, AAW40803.1, XP_502637.1, AAN39882.1, BAE57509.1, BAD93712.1, BAD93711.1, AAC98914.1 and AAF21993.1, respectively) were obtained from public databases (GenPept, PIR and UniProt). Amino acid sequences of the rubrerythrin, ferritin and hemerythrin domains were obtained from Pfam [10]. Crystal structures of hemerythrin (1HMD), rubrerythrin (1S2Z), nigerythrin (1YV1), bacterioferritin (1NF4) and several other di-iron proteins were obtained from the Protein Databank [5].

Amino acid sequences were aligned using ClustalX 1.81 [37] using the Gonnet substitution matrix [14, 15], a gap opening penalty of 10 and a gap extension penalty of 0.2. The phylogenetic trees calculated from these alignments were drawn using TREEVIEW [26]. Crystal structures were visualised using Rasmol [32] and aligned using SPDBV [16].

The hydropathy of the AOX sequence was analysed using the Eisenberg normalised consensus index [9] in which polar amino acids have a negative hydropathy (*H*) and hydrophobic amino acids have a positive *H*. The overall range of *H* in this scale is -2.5 to 1.4. The

hydrophobic moment (μ_H) of an n -residue element of secondary structure was calculated from

$$\mu_H = \sqrt{\left[\sum_{i=1}^n H_i \sin(\theta_i) \right]^2 + \left[\sum_{i=1}^n H_i \cos(\theta_i) \right]^2} \quad (1)$$

where H_i is the hydropathy of the i th residue and $\theta = 100^\circ$ for an α -helix, and is reported as the average hydrophobic moment $\langle \mu_H \rangle = \mu_H/n$ [9]. So, $\langle \mu_H \rangle$ and the average hydropathy ($\langle H \rangle = \Sigma H_i/n$) characterise secondary structure elements of particular propensities as generalised in the hydrophobic moment plot using 11 residue protein sequences of a known category.

RESULTS

A preliminary analysis of bacterial AOX amino acid sequences and a large number of di-iron sequences and di-iron protein structures prompted the hypothesis that the bacterial AOXs were more closely related to rubrerythrin, nigerythrin, hemerythrin and bacterioferritin than other di-iron proteins. While rubrerythrin, nigerythrin, hemerythrin and bacterioferritin have similar structures in which four helices surround the di-iron centre and provide the six ligands to the iron atoms in a characteristic pattern (Figure 2), the rubrerythrin domain of rubrerythrin was chosen as the basis on which to model AOX.

Hemerythrin and bacterioferritin were excluded from further consideration, largely on the basis of structure. Hemerythrin binds, but does not reduce, O_2 and each subunit has an inverted pair of hemerythrin domains and so the distribution of the iron-ligands is also inverted (Figure 2). The ferritin domain of bacterioferritin is similar to the rubrerythrin domain, but an additional haem ligand is located between two closely spaced iron ligands (Figure 2).

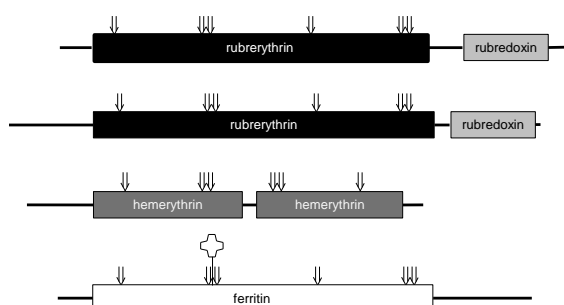


Figure 2. Summary of the domains and di-iron ligands in crystal structures of rubrerythrin (1S2Z), nigerythrin (1YV1), hemerythrin (1HMD) and bacterioferritin (1NF4) in order from top to bottom. The rectangles represent the protein domains (each of which is named according to Pfam [10]), arrows (↓) indicate the approximate positions of the ligands to the di-iron centre in each of these structures and the position of the ligand to the haem in the ferritin domain is also shown.

The rubredoxin domain of rubrerythrin and of nigerythrin contains an FeS centre, ligated between antiparallel β -strands, which is not found in AOX. The rubredoxin domain is physically distinct from the four helix bundle of the rubrerythrin domain. Therefore, the rubredoxin domain was excluded from further consideration and only the rubrerythrin domain was used in subsequent analysis.

An alignment of bacterial AOX and rubrerythrin domain amino acid sequences yielded a phylogenetic tree from which it was inferred that rubrerythrin is more similar to AOXs than it is to nigerythrin (Figure 3), therefore, rubrerythrin was chosen as a basis on which to model AOX.

Rubrerythrin crystal structures from three species are currently available: *Desulfovibrio vulgaris*, *Pyrococcus furiosus* and *Sulfolobus tokodaii*. The *S. tokodaii* rubrerythrin is apparently modified [13], therefore it was excluded and a *D. vulgaris* crystal structure (1S2Z) was chosen arbitrarily.

Bacterial and fungal AOX sequences were identified by homology with the *C. albicans* AOX amino acid sequences. These AOX sequences were highly conserved, especially in the vicinity of the E-E-E and N-E-R-M-H-L regions (Figure 4A). Although there was strong homology between the sequences, the bacterial AOXs were more distantly related to fungal AOXs than the fungal AOXs were to each other (Figure 4B). Of the bacterial AOXs, both *Vibrio* spp. and *Photobacterium* spp. are members of the *Vibrionaceae* and were closely related, whereas *Erythrobacter* sp., *Thiobacillus denitrificans* and *Novosphingobium aromaticivorans* were more distantly related to the other species.

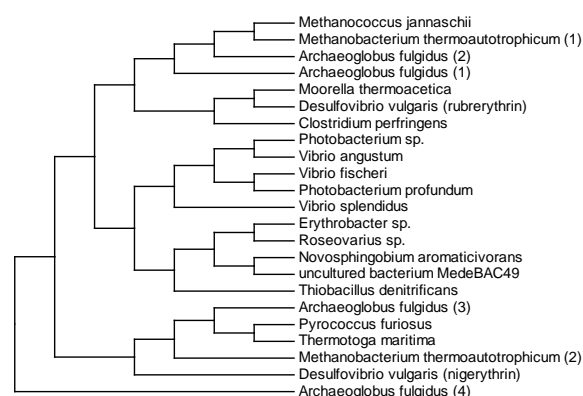


Figure 3. Phylogenetic tree derived from an alignment of selected rubrerythrin domain (from rubrerythrin and nigerythrin, obtained from Pfam [10]) and bacterial AOX sequences. The upper block of 7 species are rubrerythrins and the lower block of 6 species are nigerythrins. The central 10 species are AOXs.

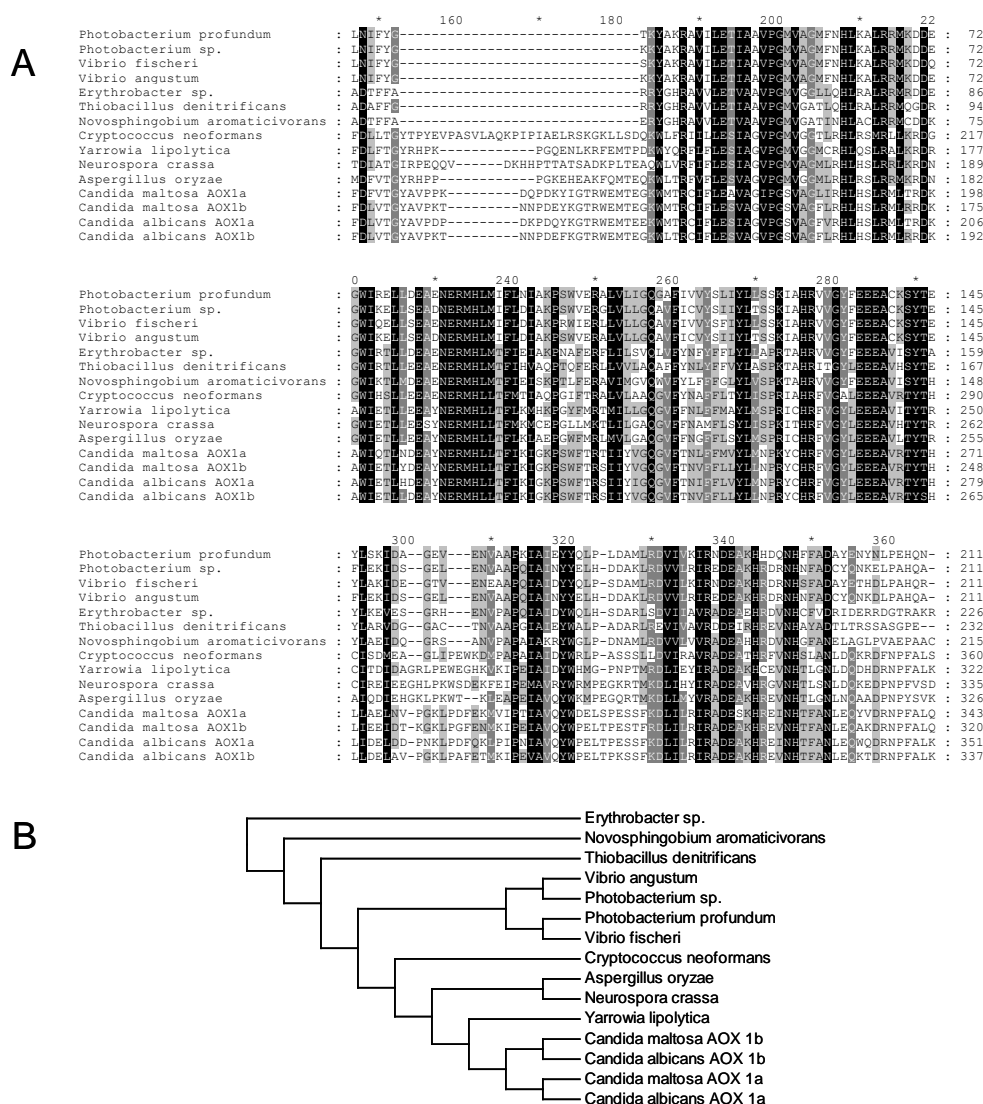


Figure 4. Protein sequence alignment of bacterial (top 7 sequences) and fungal (bottom 8 sequences) AOXs (A) and phylogenetic tree derived from it (B). Note that the N- and C-terminal sections of the alignment have been omitted.

The rubrerythrin domain amino acid sequences were poorly conserved (40–63% identity, 60–83% similarity) compared with the bacterial AOX sequences (51–98% identity, 63–99% similarity). However, the rubrerythrin domain sequences showed some homology with the bacterial AOX sequences (9–16% identity, 18–30% similarity, Figure 5). While these levels of homology between rubrerythrin and the bacterial AOXs were low, pairs of proteins having similar structures often have low sequence identity [31]. Moreover, the other common features we have identified reinforce this choice.

Identification of the putative di-iron ligands

Analysis of the crystal structure of each of several di-iron proteins (Table 1) showed that the four of the six iron ligands were associated with E-X-X-H motifs, in

which the glutamate and histidine residues ligated an iron atom. Based on the crystal structures specified in Table 1, this E-X-X-H motif could be re-summarised as [AST]-X-[DEQ]-E-X-[KR]-H. The other two iron ligands were glutamate residues located at specific distances (that is numbers of residues) from the E-X-X-H motifs. The spacing between the ligands depended on the protein, but was similar in rubrerythrin, nigerythrin and bacterioferritin (Table 1).

In the bacterial AOX sequences, such as the *Photobacterium* sp. sequence shown in Figure 5, there are two clear E-X-X-H motifs (positions 49-52 and 152-156 in the alignment) and two glutamate residues on the N-terminal side of each of these motifs (positions 10 and 104 in the alignment). The spacings are, however, more similar to those found in the more complex enzymes

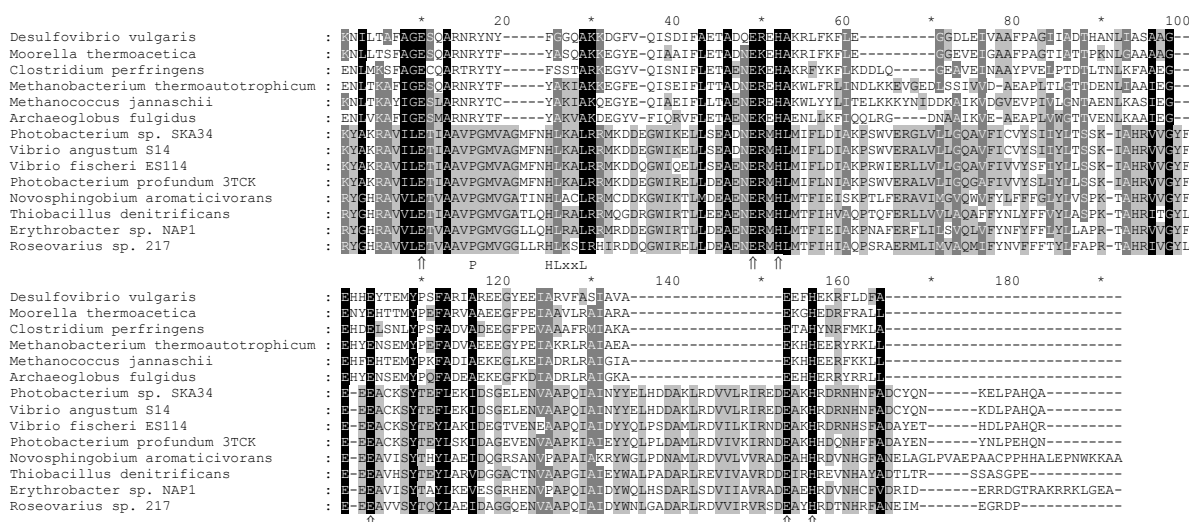


Figure 5. Partial protein sequence alignment of the rubrerythrin domain (top six sequences), originally obtained from Pfam [10], with bacterial AOXs (lower eight sequences). The alignment is shaded to emphasize similarity (using the Blossum 65 matrix), rather than identity. On the line below the alignment are indicated the location of the di-iron ligands (¶), the putative quinone binding site (HLxxL) and the conserved proline (P).

Table 1. Analysis of the spacing of the residues involved in ligating the iron atoms in the crystal structures of selected di-iron proteins. The spacing in rubrerythrin, nigerythrin and bacterioferritin is 33:41-43; 33-34, while the spacing in more complex enzymes towards the bottom of table tends to be slightly greater. D_{k-1} is not always present and is consistent with the sequence motif [AST]-X-[DEQ]-E-X-[KR]-H.

Protein	Crystal structure	Residues ligating the di-iron centre									
		D_{k-1}	E_k	H_{k+3}	E_l	H_{l+3}	E_m	E_n	$ l-n $	$ m-l $	$ k-m $
NO reductase	1YCG				83	86					
hemerythrin	1I4Y		73	77	58	54					15
nigerythrin	1YV1		149	152	73	76	115	40	33	42	34
rubrerythrin	1S2Z		128	131	53	56	94	20	33	41	34
bacterioferritin	1BCF	126	127	130	51	54	94	18	33	43	33
bacterioferritin	1NF4		132	135	56	59	99			43	
stearoyl-acyl carrier protein desaturase	1AFR	228	229	232	143	146	196	105	38	53	33
ribonucleotide reductase	1KGN		108	111	202	205	77	168	34	125	31
toluene/o-xylene monooxygenase hydroxylase	1T0Q	133	134	137	231	234					
methane monooxygenase hydroxylase	1MHY	143	144	147	243	246	209	114	129	34	65
<i>Photobacterium</i> AOX		186	187	190	85	88	138	46	39	53	49

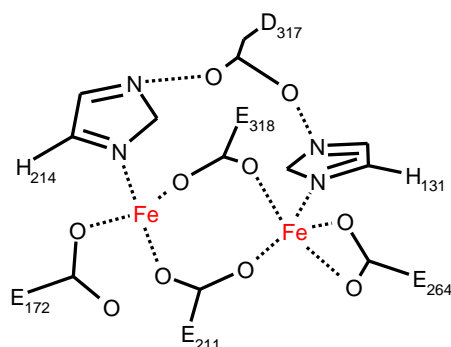


Figure 6. A model of the ligation of the di-iron centre of AOX based on the analysis of the bacterial AOX, rubrerythrin domain protein sequences and *D. vulgaris* rubrerythrin crystal structure (1S2Z). The numbering given is based on the *C. albicans* AOX1a sequence.

than those in rubrerythrin, nigerythrin and bacterioferritin, yet these sequences are less similar to AOX and were not found in the results of the BLAST searches.

The putative di-iron ligands identified were conserved in all of the fungal and bacterial AOX sequences analysed (Figures 4A and 5). Analysis of the structure of di-iron centres in the crystal structures of various di-iron proteins (Table 1), and the putative iron-binding residues yielded the following generalisations:

- a glutamate residue from each of the the E-X-X-H motifs is ligated to both of the iron atoms;
- a histidine residue from each of the E-X-X-H motifs provides a ligand to different iron atoms;
- a glutamate on the N-terminal side of each E-X-X-H motif provides the remaining ligand to the iron atoms; and
- an aspartate residue immediately to the N-terminal side of an E-X-X-H motif may polarise (or stabilise) the two histidine residues ligating the iron atoms.

Based on these generalisations and the putative iron ligands, the model of the di-iron centre shown in Figure 6 was constructed. This model shows the polarisation of the two histidine ligands (H₁₃₁ and H₂₁₄) by D₃₁₇, based on the role of a similarly placed aspartate in the crystal structures of other di-iron proteins, although it is absent from the rubrerythrin structure.

Identification of the putative quinone binding site

Fisher and Rich [11] identified a general quinone binding motif (aliphatic-X(3)-H-X(2-3)-[LTS]), but two of the three variants they identified in plant AOX sequences were absent from the *Hansenula anomala* AOX sequence [11]. Based on the alignment in Figure 4A, a better match for this motif, located just on the C-terminal side of the di-iron ligand of helix 1, was almost completely conserved among the bacterial and fungal AOX amino acid sequences (Figure 7). From this

alignment, and a more extensive analysis of quinone-binding sequences, the motif might be re-written [GA]-[MLTF]-[LFI]-[RNQ]-H-L-[HKRAQ]-[AS]-L-R, which is highly conserved among plant, fungal and bacterial AOX sequences, but absent from rubrerythrin sequences.

The rubrerythrin crystal structure has four helices in the rubrerythrin domain and the structures of these boundaries were mapped onto the alignment with the rubrerythrin domain and the bacterial AOX sequences. The putative quinone binding site identified (Figure 8, left) was located directly opposite two residues (F₂₁₅ and M₂₁₉) known to influence inhibitor sensitivity in the *A. thaliana* AOX [6]. Based on this model, UQH₂ probably binds to the putative quinone binding site by twisting around the outer surface of helix 1 due to the positions of the residues around it (Figure 8, right).

Photobacterium profundum	: LEETIARVPGMVACMFENHIALRRMKDE :	72
Photobacterium sp.	: LEETIARVPGMVACMFENHIALRRMKDE :	72
Vibrio fischeri	: LEETIARVPGMVACMFENHIALRRMKDE :	72
Vibrio angustum	: LEETIARVPGMVACMFENHIALRRMKDE :	72
Erythrobacter sp.	: LEETIARVPGMVACMFENHIALRRMKDE :	86
Thiobacillus denitrificans	: LEETIARVPGMVACMFENHIALRRMKDE :	94
Novosphingobium aromaticivorans	: LEETIARVPGMVACMFENHIALRRMKDE :	75
Cryptococcus neoformans	: LEETIARVPGMVACMFENHIALRRMKDE :	217
Yarrowia lipolytica	: LEETIARVPGMVACMFENHIALRRMKDE :	177
Neurospora crassa	: LEETIARVPGMVACMFENHIALRRMKDE :	189
Aspergillus oryzae	: LEETIARVPGMVACMFENHIALRRMKDE :	182
Candida maltosa_AOX1a	: LEETIARVPGMVACMFENHIALRRMKDE :	198
Candida maltosa_AOX1b	: LEETIARVPGMVACMFENHIALRRMKDE :	175
Candida albicans_AOX1a	: LEETIARVPGMVACMFENHIALRRMKDE :	206
Candida albicans_AOX1b	: LEETIARVPGMVACMFENHIALRRMKDE :	192

Figure 7. Alignment of the C-terminal side of the di-iron ligand in helix 1 (see below) indicated by ↑ under the first conserved E in the alignment) showing the quinone-binding motif (aliphatic-X(3)-H-X(3)-L, where the α in the motif denotes the aliphatic residue).

Hydropathy analysis of the putative helices

The hydropathy analysis was carried out to assist in determining how AOX might be located relative to the membrane and to differentiate between the interfacial and integral models (Figure 1). The helices observed in the *D. vulgaris* rubrerythrin structure (1S2Z) were mapped onto the alignment of bacterial AOXs and rubrerythrin sequences. The *Photobacterium* sp. AOX sequence (Figure 5) was used to specify the four AOX helical sequences, from which $\langle\mu_H\rangle$ and $\langle H\rangle$ were calculated in the two ways: (1) a sliding 11-residue window was moved through each helical sequence to identify putatively amphipathic sub-sequences, and (2) an 18-residue sequence including the most amphipathic or most hydrophobic regions of each sequence was analysed to summarise the properties of the region (Figure 9).

The central 18 residues of helix 1 are hydrophobic and would be classified by Eisenberg [9] as a transmembrane helix, whereas the N- and C-terminal portions of this helix are amphipathic ($\langle\mu_H\rangle = 0.48 \text{ residue}^{-1}$ and $\langle\mu_H\rangle = 0.57 \text{ residue}^{-1}$, respectively). This implies that each end of the helix is only partially embedded in the membrane while the central section is completely embedded. This hypothesis is partly supported by the presence of a proline (P) in the centre of the hydrophobic region which

is often associated with curvature of helices [27]. This proline (P) residue is conserved among the bacterial and fungal AOX sequences, but not in the rubrerythrin sequences.

Helix 2 is within the ‘globular’ region of the Eisenberg [9] hydrophobic moment plot. Like the hydrophobic region of helix 1, this helix is not especially amphipathic because of the distribution of charged residues like D, E

and R. However, the central 11-mer (WIRELLDEAEN) has $\langle\mu_H\rangle = 0.66$ and $\langle H\rangle = -0.14$, indicating only limited amphipathicity. This implies that the helix is likely to be located outside the membrane. The E and H in the N-E-R-M-H-L motif are completely conserved among the bacterial and fungal AOX and rubrerythrin sequences and are putative ligands to the di-iron centre (E_{211} and H_{214} of the *C. albicans* sequence).

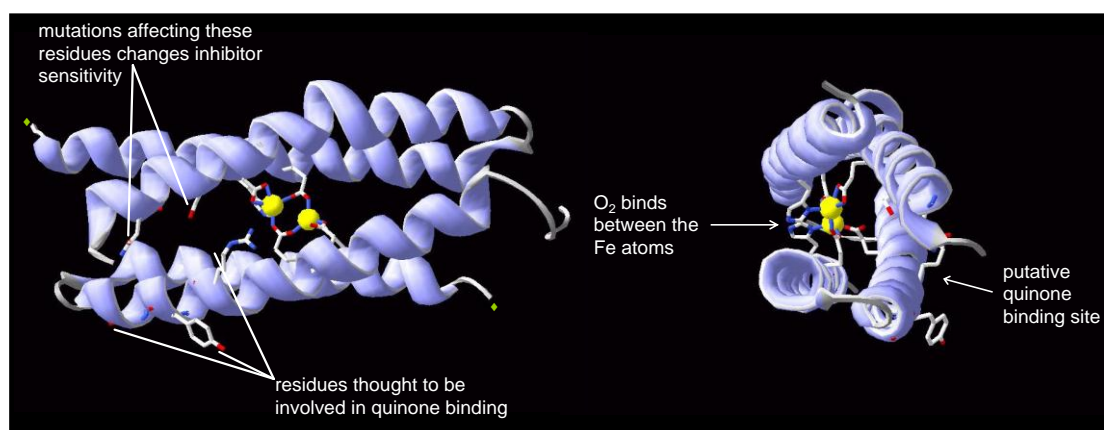


Figure 8. Model of the structure of AOX, side view (left) and head-on view (right), based on the rubrerythrin crystal structure (1S2Z) and the *C. albicans* AOX1a sequence.

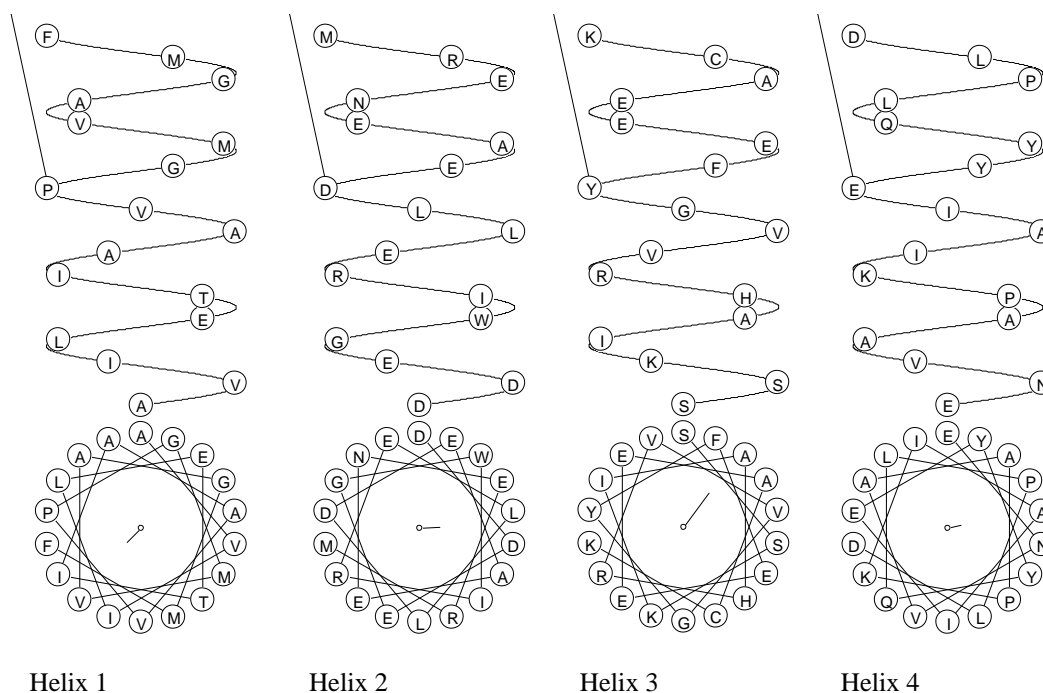


Figure 9. The hydrophobic moment analysis of the four helices of the AOX model. The upper plot is the helix viewed from the side (N-terminus at the bottom) and the lower plot is the helix viewed from the N-terminal end (the upper plot is rotated 90° around a horizontal axis in the plane of the page). Note that the positions of the residues in the upper and lower plots correspond in horizontal distribution. The direction of the line in the centre of each lower plot points towards the hydrophobic face of the helix and the length indicates the relative hydrophobic moment ($\langle\mu_H\rangle$). The relative orientation of the four helices does not reflect their orientation in the model structure. For helices 1 to 4 $\langle\mu_H\rangle = -0.21, 0.21, 0.45$ and 0.14 residue $^{-1}$, respectively, and $\langle H\rangle = 0.68, -0.34, -0.08$ and 0.17 residue $^{-1}$, respectively.

The N-terminal 18 residues of helix 3 are amphipathic, but the central 11-mer of this sequence (SKIAHRVVGYYF) has $\langle\mu_H\rangle = 0.59$ residue⁻¹ and $\langle H\rangle = 0.14$ residue⁻¹, indicating that this helix is within the 'surface' region of the Eisenberg [9] hydrophobic moment plot. The C-terminus of this helix is hydrophilic. The E-E-E motif is completely conserved among the fungal and bacterial AOX sequences, but not among the rubrerythrin sequences (these have E-[HN]-[DHYF]-E aligned with E-E-E). The third glutamate is the putative ligand to the di-iron centre. The N-terminus of this helix is likely to be partially embedded in the membrane.

Helix 4 is clearly only slightly hydrophobic and not amphipathic. The D-E-A-K-H motif contains the two completely conserved residues E and H which are putative ligands to the di-iron centre. This helix probably lies outside the membrane.

DISCUSSION

The crystal structure of rubrerythrin was used as a basis on which to construct a simple model of AOX. In addition to the overall structure of the protein, putative quinone binding site and di-iron ligands were identified. It is difficult to obtain data that support this model rather than either of the other two models that have been proposed (Figure 1). However, three considerations do support it. First, the putative quinone binding site is located opposite the sites of mutations (F₂₁₅, M₂₁₉ or G₃₀₃) that have previously been shown (in *A. thaliana*) to alter the sensitivity of AOX to SHAM [6]. If modification of these residues interferes in some way with the binding of SHAM, then they could be adjacent to the SHAM binding site. Second, the putative quinone binding site and the di-iron centre are close together, consistent with efficient electron transfer between them. Finally, Albury *et al.* [1] reported that a modification of several of the putative di-iron ligands such as E217A yielded an inactive enzyme.

This model prompts the suggestion that the enzyme is a peripheral protein in which part of one helix is embedded in the membrane and much of the remainder of it is located outside the membrane. If AOX is a di-iron protein in which the di-iron centre is ligated within a four-helix bundle, like other members of this family, and if the enzyme is an integral protein, all of the four helices should span the bilayer to maintain the pattern of ligation of the di-iron centre. The hydrophobic portion of helix 1 might be long enough to span the bilayer [23], but none of the other helices are hydrophobic as would be required to be consistent with the integral protein model (Figure 1A) of Moore *et al.* [25, 33]. Helices 2 and 4 are hydrophilic, inconsistent with a model in which all four helices span the bilayer, unless the

enzyme forms an oligomer in which they are located towards the centre. While the plant enzyme is known to form a dimer, fungal enzymes appear to lack this feature [38].

The interfacial model (Figure 1B) of Andersson and Nordlund [3] implies that AOX is partially embedded in the membrane. In order to justify this model, there should be (1) at least one hydrophobic helix embedded in the membrane, perhaps an amphipathic helix located at the membrane surface and at least one hydrophilic helix located outside the membrane; or (2) a consistent pattern of amphipathicity and hydrophilicity implying that a portion of the protein is located within the membrane. The former extreme is possible if the protein lies parallel to the membrane surface, while the latter is feasible if the protein is not approximately perpendicular to the membrane surface.

The hydropathy analysis and the putative quinone binding site imply that a combination of the two extremes is more likely. The central region of helix 1 is hydrophobic and the N- and C-terminal regions are amphipathic. As helix 1 is probably bent, it can be visualised as bending out of the membrane such that both ends of the helix are partly embedded in the membrane, and the C-terminus of the helix in which the putative quinone binding site is located would be accessible to the quinone. Helix 3 is partly amphipathic, therefore, the N-terminus of the helix is probably located at the membrane surface, allowing the di-iron ligands in helices 1 and 3 to be aligned (the [last] glutamates in the V-I-L-E-T and E-E-E motifs). Helices 2 and 4 are hydrophilic, providing the (D)-E-X-X-H motifs of the other di-iron ligands.

The model we have developed is summarised in Figure 10. The di-iron centre (Figure 6) is ligated by specific residues located in a four helix bundle (Figure 8) parts of which are embedded in the inner mitochondrial membrane. This is inconsistent with the transmembrane model (Figure 1A), but shares some features with the interfacial model (Figure 1B). However, the details of the arrangement and shape of the helices, the identification of the conserved proline in helix 1, the location of the putative quinone binding site in relation to the di-iron centre and the specific ligands to the iron atoms differ from those specified in [3].

CONCLUSIONS

While this is the first time such a detailed model of AOX has been constructed, the hydropathy analysis of AOX and position of the putative quinone binding site support the general model proposed by Andersson and Nordlund [3], in that both models predict a peripheral protein, although the models differ in several details. The location of the putative binding site opposite sites of

mutations that have been known to alter SHAM sensitivity are consistent with their proximity to the SHAM binding site. The putative quinone binding motif should be analysed in more detail and the quality of the structural detail of the current model is yet to be exhaustively checked.

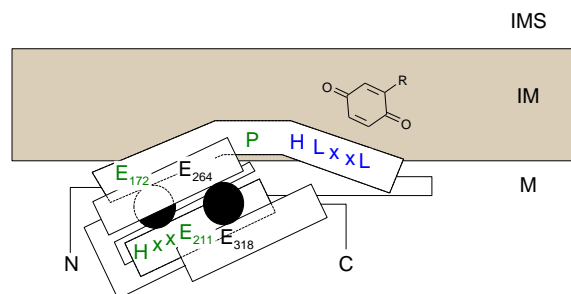


Figure 10. A model of the structure of AOX based on the analysis of the bacterial AOX, rubrerythrin domain protein sequences and *D. vulgaris* rubrerythrin crystal structure (1S2Z). The curvature and relative length of helix 1 around the conserved proline residue (P) is exaggerated. The numbering given is based on the *C. albicans* AOX1a sequence as in Figure 6. The filled circles represent the iron atoms and the rectangles represent the proposed helical regions. The putative quinone-binding motif is indicated (HLxxL) in blue and the ligands to the di-iron centre are also indicated (although H₁₃₁ is omitted). The quinone in the membrane is not intended to be a correct representation of UQ. IMS – intermembrane space; IM – inner membrane; M – matrix.

REFERENCES

- [1] Albury, M. S., C. Affourtit, P. G. Crichton and A. L. Moore (2002) Structure of the plant alternative oxidase. Site-directed mutagenesis provides new information on the active site and membrane topology. *J Biol Chem*, 277(2): 1190-1194
- [2] Allen, J. P., G. Feher, T. O. Yeates, H. Komiya and D. C. Rees (1988) Structure of the reaction center from *Rhodobacter sphaeroides* R-26: protein-cofactor (quinones and Fe²⁺) interaction. *Proc Natl Acad Sci USA*, 85(22): 8487-8491
- [3] Andersson, M. E. and P. Nordlund (1999) A revised model of the active site of alternative oxidase. *FEBS Lett*, 449(1): 17-22
- [4] Atta, M., K. K. Andersson, R. Ingemarson, L. Thelander and A. Gräslund (1995) EPR studies of mixed-valent [Fe^{II}Fe^{III}] clusters formed in the R2 subunit of ribonucleotide reductase from mouse or herpes simplex virus: mild chemical reduction of the diferric centers. *J Am Chem Soc*, 116: 6429-6430
- [5] Berman, H. M., J. Westbrook, Z. Feng, G. Gilliland, T. N. Bhat, H. Weissing, I. N. Shindyalov and P. E. Bourne (2000) The Protein Data Bank. *Nucleic Acids Res*, 28: 235-242
- [6] Berthold, D. A. (1998) Isolation of mutants of the *Arabidopsis thaliana* alternative oxidase (ubiquinol:oxygen oxidoreductase) resistant to salicylhydroxamic acid. *Biochim Biophys Acta*, 1364(1): 73-83
- [7] Berthold, D. A., N. Voevodskaya, P. Stenmark, A. Gräslund and P. Nordlund (2002) EPR studies of the mitochondrial alternative oxidase. Evidence for a diiron carboxylate center. *J Biol Chem*, 277(46): 43608-43614
- [8] Deisenhofer, J., O. Epp, K. Miki, R. Huber and H. Michel (1984) X-ray structure analysis of a membrane protein complex. Electron density map at 3 Å resolution and a model of the chromophores of the photosynthetic reaction center from *Rhodospseudomonas viridis*. *J Mol Biol*, 180(2): 385-398
- [9] Eisenberg, D., R. M. Weiss and T. C. Terwilliger (1984) The hydrophobic moment detects periodicity in protein hydrophobicity. *Proc Natl Acad Sci USA*, 81: 140-144
- [10] Finn, R. D., J. Mistry, B. Schuster-Böckler, S. Griffiths-Jones, V. Hollich, T. Lassmann, S. Moxon, M. Marshall, A. Khanna, R. Durbin, S. R. Eddy, E. L. L. Sonnhammer and A. Bateman (2006) Pfam: clans, web tools and services. *Nucleic Acids Res*, 34: D247-D251
- [11] Fisher, N. and P. R. Rich (2000) A motif for quinone binding sites in respiratory and photosynthetic systems. *J Mol Biol*, 296: 1153-1162
- [12] Fox, B. G., K. S. Lyle and C. E. Rogge (2004) Reactions of the diiron enzyme stearyl-acyl carrier protein desaturase. *Acc Chem Res*, 37(7): 421-429
- [13] Fushinobu, S., H. Shoun and T. Wakagi (2003) Crystal structure of sulerythrin, a rubrerythrin-like protein from a strictly aerobic archaeon, *Sulfolobus tokodaii* strain 7, shows unexpected domain swapping. *Biochem*, 42: 11707-11715
- [14] Gonnet, G. H., M. A. Cohen and S. A. Benner (1992) Exhaustive matching of the entire protein sequence database. *Science*, 256: 1443-1445
- [15] Gonnet, G. H., M. A. Cohen and S. A. Benner (1994) Analysis of amino acid substitution during divergent evolution: the 400 by 400 dipeptide substitution matrix. *Biochem Biophys Res Commun*, 199: 489-496
- [16] Guex, N. and M. C. Peitsch (1997) SWISS-MODEL and the Swiss-PdbViewer: an environment for comparative protein modeling. *Electrophoresis*, 18(15): 2714-2723
- [17] Harrison, P. M., P. D. Hempstead, P. J. Artymiuk and S. C. Andrews (1998) Structure-function relationships in the ferritins. *Metal Ions in Biol Systems*, 35: 435-477
- [18] Jin, S., D. M. Kurtz, Jr., Z. J. Liu, J. Rose and B. C. Wang (2004) Displacement of iron by zinc at the diiron site of *Desulfovibrio vulgaris* rubrerythrin: X-ray crystal structure and anomalous scattering analysis. *J Inorg Biochem*, 98(5): 786-796
- [19] Kurtz, D. M., Jr. (1997) Structural similarity and functional diversity in diiron-oxo proteins. *J Biol Inorg Chem*, 2(2): 159-167
- [20] Lombardi, A., C. M. Summa, S. Geremia, L. Randaccio, V. Pavone and W. F. DeGrado (2000) Retrostructural analysis of metalloproteins: Application to the design of a minimal model for diiron proteins. *Proc Natl Acad Sci USA*, 97(12): 6298-6305

- [21] Macedo, S., C. V. Romão, E. Mitchell, P. M. Matias, M. Y. Liu, A. V. Xavier, J. LeGall, M. Teixeira, P. Lindley and M. A. Carrondo (2003) The nature of the di-iron site in the bacterioferritin from *Desulfovibrio desulfuricans*. *Nature Struct Biol*, 10(4): 285-290
- [22] McCormick, J. M., R. C. Reem and E. I. Solomon (1991) Chemical and spectroscopic studies of the mixed-valent derivatives of the non-heme iron protein hemerythrin. *J Am Chem Soc*, 113(24): 9066-9079
- [23] McLean, L. R., K. A. Hagaman, T. J. Owen and J. L. Krstenansky (1991) Minimal peptide length for interaction of amphipathic α -helical peptides with phosphatidylcholine liposomes. *Biochem*, 30(1): 31-37
- [24] Minagawa, N., S. Sakajo, T. Komiyama and A. Yoshimoto (1990) Essential role of ferrous iron in cyanide-resistant respiration in *Hansuela anomala*. *FEBS Lett*, 267: 114-116
- [25] Moore, A. L., A. L. Umbach and J. N. Siedow (1995) Structure-function relationships of the alternative oxidase of plant mitochondria: a model of the active site. *J Bioenerg Biomembr*, 27(4): 367-377
- [26] Page, R. D. M. (1996) TREEVIEW: An application to display phylogenetic trees on personal computers. *Comput Appl Biosci*, 12: 357-358
- [27] Piela, L., G. Némethy and H. A. Scheraga (1987) Proline-induced constraints in α -helices. *Biopolymers*, 26: 1587-1600
- [28] Pierik, A. J., R. B. Wolbert, G. L. Portier, M. F. Verhagen and W. R. Hagen (1993) Nigerythrin and rubrerythrin from *Desulfovibrio vulgaris* each contain two mononuclear iron centers and two dinuclear iron clusters. *Eur J Biochem*, 212(1): 237-245
- [29] Ravi, N., B. C. Prickril, D. M. Kurtz, Jr. and B. H. Huynh (1993) Spectroscopic characterization of ^{57}Fe -reconstituted rubrerythrin, a non-heme iron protein with structural analogies to ribonucleotide reductase. *Biochem*, 32(33): 8487-8491
- [30] Rhoads, D. M. and L. McIntosh (1991) Isolation and characterization of a cDNA clone encoding an alternative oxidase protein of *Sauromatum guttatum* (Schott). *Proc Natl Acad Sci USA*, 88(6): 2122-2126
- [31] Rost, B. (1997) Protein structures sustain evolutionary drift. *Folding Design*, 2(3): S19-S24
- [32] Sayle, R. A. and E. J. Milner-White (1995) RASMOL: biomolecular graphics for all. *Trends Biochem Sci*, 20(9): 374
- [33] Siedow, J. N., A. L. Umbach and A. L. Moore (1995) The active site of the cyanide-resistant oxidase from plant mitochondria contains a binuclear iron center. *FEBS Lett*, 362: 10-14
- [34] Stenkamp, R. E., L. C. Sieker and L. H. Jensen (1984) Binuclear iron complexes in methemerythrin and azidomethemerythrin at 2.0 Å resolution. *J Am Chem Soc*, 106: 618-622
- [35] Stenkamp, R. E., L. C. Sieker, L. H. Jensen, J. D. McCallum and J. Sanders-Loehr (1985) Active site structures of deoxyhemerythrin and oxyhemerythrin, *Proc Natl Acad Sci USA*, 82(3): 713-716
- [36] Summa, C. M., M. M. Rosenblatt, J. K. Hong, J. D. Lear and W. F. DeGrado (2002) Computational *de novo* design, and characterization of an A_2B_2 diiron protein. *J Mol Biol*, 321(5): 923-938
- [37] Thompson, J. D., T. J. Gibson, F. Plewniak, F. Jeanmougin and D. G. Higgins (1997) The ClustalX windows interface: flexible strategies for multiple sequence alignment aided by quality analysis tools. *Nucleic Acids Res*, 24: 4876-4882
- [38] Umbach, A. L. and J. N. Siedow (2000) The cyanide-resistant alternative oxidases from the fungi *Pichia stipitis* and *Neurospora crassa* are monomeric and lack regulatory features of the plant enzyme. *Arch Biochem Biophys*, 378(2): 234-245